


Research Article

Eco-Speed Harmonization with Partially Connected and Automated Traffic at an Isolated Intersection

Zhen Kang,¹ Lianhua An ,¹ Jintao Lai,¹ Xiaoguang Yang,¹ and Wensheng Sun²

¹Key Laboratory of Road and Traffic Engineering of the Ministry of Education, Tongji University, Shanghai 201804, China

²Schaeffler Trading (Shanghai) Co., Ltd., No. 1 Antuo Road, Anting, Jiading District, Shanghai 201804, China

Correspondence should be addressed to Lianhua An; an_lianhua@163.com

Received 4 July 2023; Revised 25 August 2023; Accepted 25 September 2023; Published 9 October 2023

Academic Editor: Jing Zhao

Copyright © 2023 Zhen Kang et al. This is an open access article distributed under the Creative Commons Attribution License, which permits unrestricted use, distribution, and reproduction in any medium, provided the original work is properly cited.

This paper proposed an eco-speed harmonization method at intersections. It is able to reduce carbon emissions by controlling partially connected and automated traffic and signal timing. It has the following features: (i) traffic emission reduction enhancement at various demand levels; (ii) traffic emission achievement while improving the mobility of entire traffic at intersections; (iii) enhanced traffic emission reduction with the help of a small portion of connected and automated vehicles; and (iv) potential implementations in the near future. To validate the effectiveness, the proposed method is evaluated against a state-of-the-art strategy. Sensitivity analysis is conducted under various demand levels and market penetration rates (MPRs) of connected and automated vehicles (CAVs). The result shows that the proposed method outperforms and has the benefits of traffic emission reduction, throughput improvement, and stop frequency reduction. The proposed method demonstrates consistent performance across all demand levels and CAVs' MPR. The proposed approach can achieve a reduction in emissions ranging from 4% to 61%, an average increase in throughput of around 14.91%, and a decrease in the stop frequency of at least 26%. This provides the foundation for future CAVs-based eco-approaching strategies.

1. Introduction

Greenhouse gas emissions are a worldwide issue that demands urgent attention. According to the International Energy Agency (IEA), the transport sector is responsible for 25–30% of a country's total carbon emissions [1]. Among various modes of transportation, road transportation alone accounts for approximately 80% of emissions. Consequently, there is an urgent need for effective measures to curb emissions in road transportation.

Eco-driving technology is an important way to reduce emissions. Its main idea is to achieve emission reduction by decreasing stops of the vehicle at signalized intersections. Specifically, it is realized by changing the speed of the vehicle to make it go through the intersection at green lights. In urban roads, there are many practical applications [2–9]. The ecological speed advice is sent to vehicles through the navigation application on the vehicle terminal. However, due to the driving randomness of human-driven vehicles

(HVs), speed advice is not always strictly followed. This may lead to the stopping of vehicles at the intersection. The benefit brought by eco-driving strategies would be impaired.

Fortunately, the emerging connected and automated vehicle (CAV) technologies bring possibilities to solve the issue of driving randomness. CAVs can precisely execute the suggested speed. This brings great potential to reduce greenhouse gas emissions at intersections. In the beginning, many studies have developed CAVs-based eco-approach strategies in pure connected and automated traffic [10–16]. In these studies, the CAVs' advantage in precise execution is taken off. It achieves good performance on carbon emissions in pure connected and automated traffic. However, achieving a 100% market penetration rate (MPR) for CAVs is not expected until the 2060s [17]. This implies that a mixed traffic environment consisting of both CAVs and HVs will exist for a long time. Therefore, it is crucial to develop eco-driving technologies that are compatible with partially connected and automated traffic.

Recently, many ecological driving strategies have been proposed for partially connected and automated traffic [18, 19]. Most of these strategies either focus on controlling one CAV under the influence of the front HVs [14–17] or forming a platoon in mixed traffic [13, 16, 20]. The former desperates to control a CAV to catch the green lights. The control trajectory integrates lane-changing and speed-changing. The latter controls the platoon with a leading CAV. Both of them have shown their potential for carbon emissions.

However, the existing methods have limitations.

Firstly, the existing methods are weak in emission reduction assurance in various traffic demands. Day-to-day demand variations are common existence in the urban city. Most eco-driving strategies demonstrate good performance under limited conditions, such as conditions of low traffic saturation or demand level [16]. The performance under high demand levels cannot be assured. These ecological strategies primarily rely on the precise control of the trajectories of vehicles to achieve benefits. The control strategy includes the change of speed and lane changes [21, 22]. However, ensuring the precise execution of vehicles in congested traffic conditions is challenging. The imprecise control of vehicles would lead to poor performance of emission reduction.

Secondly, the existing methods overlook the need for mobility improvement while ensuring emission reduction. The improvement of mobility at intersections is of great importance. This is because mobility is a key index for representing the service level of the traffic for the city. Improving mobility is a key goal for traffic management. However, the existing eco-approach methods are unable to balance the improvement of mobility and emission reduction. They are mainly focused on enhancing the benefit of some portion of vehicles. This may sometimes damage the benefit of the other surrounding vehicles [16, 23–26]. In these studies, emission reduction is achieved by reducing the stops of controlled vehicles. Considering such a situation that the controlled vehicles conduct lane changes to go through the intersection, with the eco-driving control strategy, the controlled vehicle is able to catch the green light and avoid a stop. This is helpful for the mobility and emission reduction of the controlled vehicle. However, due to the frequent lane changes and speed changes of the controlled vehicle, other surrounding vehicles may suffer the benefit of loss of mobility and emission reduction. Therefore, the mobility of the entire traffic is hardly able to be ensured.

Thirdly, the existing eco-approach methods show a limitation at the early stage of CAV roll-out (with low MPR). In most of the existing methods, it requires CAVs to cut through traffic to form a platoon. The requirements for platoon formation are strict. Each platoon is required to be led by a CAV. All CAVs must be positioned ahead of each HV within the platoon [27]. However, under low MPR, platoon formation is not always achievable. Especially when CAVs are much less than HVs, it is of great difficulty for CAVs to cut through traffic to form a platoon or become a leading vehicle of each platoon [25, 28]. This impedes the method in the practical application. In this situation, the benefit of emission reduction brought by CAVs is also impaired a lot.

Fourthly, the existing method applications are weak in practicality. The limitation of the application lies in its high demand for computation power. The solution of the eco-driving strategy requires a large amount of computational power. It includes multi-task solving: state prediction of surrounding vehicles, decision making, trajectory planning, and control [10, 16, 21, 25, 29–31]. Due to the requirement for high-frequency updates on control information, each task solving consumes quite a lot of computational power. Although some studies develop a distributed solution to reduce the computational burden of the onboard unit [32], it is still cost-ineffective to have an onboard unit providing such high computation resources.

Given the shortcomings of the existing eco-approach applications, this paper proposes an enhanced eco-approach method. It coordinates the optimization of signal and vehicles' speed under partially connected and automated traffic. It bears the following features:

- (i) Enhancing carbon emission reduction at various demand levels
- (ii) Improving mobility of entire traffic at intersection
- (iii) Enhancing carbon emission reduction with the help of a small portion of connected and automated vehicles
- (iv) Potential implementations in the near future

This paper is organized as follows. Section 2 presents the control mechanism. Section 3 presents the problem description. Section 4 presents the control methods, including traffic status prediction module, signal control module, and CAV speed harmonization module. Section 5 evaluates the performance of proposed method. Section 6 provides the conclusions and future works.

2. Control Mechanism

The goal of the proposed controller is to reduce emissions for vehicles approaching an isolated signalized intersection. The control strategy is able to balance the improvement of emission reduction and mobility of entire traffic at intersections. There are three highlights of this proposed controller.

2.1. Controlling the Entire Connected and Automated Traffic as a Whole. To address the issue of the computation burden, the control object is transformed from individual CAVs to the entire connected and automated traffic as a whole. The control variable is reduced to a one-dimension variable (desired speed of CAVs). The dimension of the control variable is not increasing with the number of CAVs. This helps to avoid computing burden issues.

2.2. Cooperation of Demand Management and Signal Control. The proposed speed harmonization method aims to achieve a balance between demand and supply. The demand control is to adjust flow through CAV speed harmonization. In the speed harmonization module, the desired speed for CAVs is

determined based on the signal status. This design aims to achieve an optimal match between the arrival demands and the signal status, ultimately reducing the average frequency of stops. The supply control is the throughput adjustment by signal control. The signal control module switches the signal control status based on the traffic flow state. It aims to ensure the maximum throughput at the intersection.

2.3. Enhancing Carbon Emission Reduction While Improving Mobility. By introducing a traffic status prediction model, the impact of speed harmonization strategy on the mobility of the entire traffic is considered in advance. The prediction model is developed based on “phantom density” (defined on page 8). The phantom density describes how the density changes with CAVs’ desired speed over time. It reveals the current influence of CAVs’ desired speed on future traffic states. The signal lights prioritize the release of phase with a high phantom density as it indicates a high traffic demand and tightly formed traffic flow. This design helps to reduce emissions and maximize the mobility of the entire traffic by reducing vehicle stops.

3. Problem Statements

The studied scenario is an isolated signalized intersection, as shown in Figure 1. It is a typical 4-leg, 3-lane (in each direction) signalized intersection. The three lanes serve different purposes: a through/left-turning lane, a through lane, and a through/right-turning lane. The signal timing plan is predetermined and consists of either 2 or 4 signal phases. The signal phases are not optimized variables. Each phase is divided into an effective green interval and a clearance time (including yellow and all-red time). The clearance time is predesigned and fixed within the system. The proposed method only modifies the green duration of each phase during the optimization process, without a fixed cycle duration. The maximum and minimum green time schemes comply with standard signal design practices.

In this study, the scenario operates in a partially connected and automated traffic environment. The vehicles in this scenario are CAVs and connected human-driving vehicles (CHVs). All vehicles have the ability to communicate with roadside units through Vehicle-to-Vehicle (V2V) and Vehicle-to-Infrastructure (V2I) technologies in real time. This means that the vehicles can obtain real-time signal timing information. The roadside control center can obtain real-time vehicle status information (position, speed). The control segment is from the upstream segment to the location before the forbidden Lane Changing Zone, which is usually a few hundred meters. In the control segment, CAVs are scattered among CHVs with no platoon formed. Desired speed commands are provided from a control center to CAVs with an update frequency of Δt . When CAVs travel on a road segment under control, all CAVs receive an identical desired speed command.

4. Methods

This section provides a detailed representation of the proposed method, including the control structure, signal control module, and CAV speed harmonization module.

4.1. Parameters and Notations. The notations and parameters utilized hereafter are defined in Table 1.

4.2. Control Structure. Figure 2 illustrates the control structure, which includes the traffic status prediction module, signal control module, and speed harmonization module.

The signal control module is adjusted according to the phantom density of the traffic. It is predesigned with an optimal signal timing configuration during time interval $(m + 1)$. Details on the signal control method are presented in Section 4.4.

CAV speed harmonization module is adjusted according to the information of signal timing and phantom density. It calculates the desired speed for CAVs and outputs a series of control profiles of CAVs. The output information includes the future speed decision of CAVs. The implementation of these control profiles obeys a rolling-horizon rule. Only the first step of the profiles is executed by CAVs.

The first step of the control command is to output it for implementation by CAVs. Furthermore, it predicts the desired speed for CAVs during time interval $(m + 2)$ and outputs it to the traffic status prediction module. Section 4.5 will present more detailed information on this process. Details on the CAV speed harmonization method are presented in Section 4.4.

4.3. Traffic Status Prediction Module. The traffic status is characterized by the density level. The density is commonly utilized to describe the congestion level of traffic status. Some studies suggest that preventing the density from reaching the critical zone is crucial for effective control [33, 34]. Density serves as an important criterion for traffic control. Building upon this idea, the objective of the traffic status prediction module is to predict the density change. This forecasting holds significant value as it provides a realistic representation of the dynamic changes in road traffic conditions resulting from CAVs’ speed change. That is, the proposed prediction model is actually to describe the change of density under the influence of CAVs’ speed change. This serves as the foundation for the design of the proposed strategy.

The coordination between CAVs is influenced by signal timing. During the red interval, CAVs slow down in advance to reduce the number of stops at intersections. During the green interval, CAVs operate at a maximum acceleration to catch the green light. Here the traffic status prediction model is piecewise based on the signal timing. Details are as follows.

- (i) Situation 1: when it is during the red interval.

During the red interval, the speed of traffic flow changes due to CAVs’ deceleration and

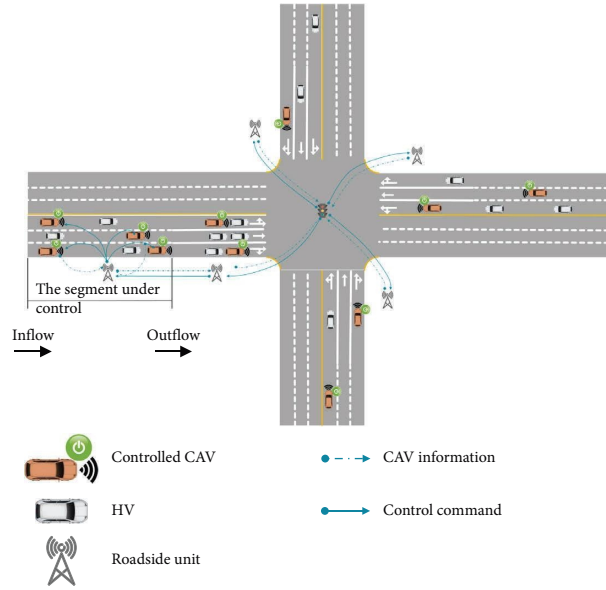


FIGURE 1: Illustration of the scenario.

TABLE 1: Notations and parameters.

Notations	Explanation	Unit
\bar{k}	The phantom density of the entire traffic flow (defined on page 8)	pcu/km
γ_m	The portion of vehicles under the influence of CAVs' speed change at update time interval	
ξ_m	The penetration rate of CAVs at update time interval m	
D	The number of phases	
v_m	The average speed of all vehicles during the update time interval m	m/s
u_m	The desired speed of CAVs during update time interval m	m/s
v_a	The speed of the preceding vehicle	m/s
v_b	The speed of the following vehicle	m/s
v_m^D	The desired speed of CAVs in phase D during the update time interval m	m/s
v_{rl}	The road speed limit	m/s
v_f	The free-flow speed on the road segment	m/s
w	The dissipation speed of the rarefaction wave	m/s
Δv_m^D	The average speed change for CAVs in phase D during the update time interval m	m/s ²
$\Delta v_{m_max}^D$	The maximum speed change in phase D during the update time interval m	m/s ²
a_{min}	The minimum acceleration	m/s ²
a_{max}	The maximum acceleration	m/s ²
k_m	The density of the entire traffic flow during update time interval m	pcu/km
\bar{k}_m	The phantom density of the entire traffic flow during update time interval m (defined on page 9)	pcu/km
\bar{k}_{max}	The maximum phantom density at the intersection	pcu/km
k_c	The critical density	pcu/km
k_{jam}	The jam density	pcu/km
k_m^G	The density of the current green phase at time interval m	pcu/km
\bar{k}_m^D	The phantom density of phase D during the update time interval m	pcu/km
$k_{m_b}^D$	The buffer density for phase switching of the phase D during update time interval m (defined on page 9)	pcu/km
q_c	The maximum flow at the critical density	pcu/h
T	The length of time that the average speed approaches CAVs' desired speed	s
T_m^G	The duration of the green interval during the update time interval m	s
T_m^R	The duration of the red interval during the update time interval m	s
Δt	The update time interval	s
t_{LC}	The average lane-changing duration	s
t_m^i	The travel time of vehicle i on the control segment during time interval $[m-1, m]$	s

TABLE 1: Continued.

Notations	Explanation	Unit
t_{clear}	The clearance time to clear the vehicles passing the stop line at the end of the effective green time	s
G_{max}	The maximum duration of the green interval	s
G_{min}	The minimum duration of the green interval	s
τ	The driver's response time	s
H_s	The safe time headway	s
t_s	The start-up time of the last vehicle in the queue	s
L	The length of the control segment	m
S_{min}	The safe following distance	m
\bar{S}_m^D	The average headway distance of phase D during time interval m	m
Δ_{safe}	The safety buffer distance (defined on page 15)	m
\bar{h}_s	The average stopping distance of vehicles when queuing	m
\bar{l}	The average length of vehicles	m
L	The length of the controlled road segment	m
N_q	The number of queued vehicles in the current lane	pcu
N_m	The number of vehicles on the controlled road segment during time interval $[m - 1, m]$	pcu

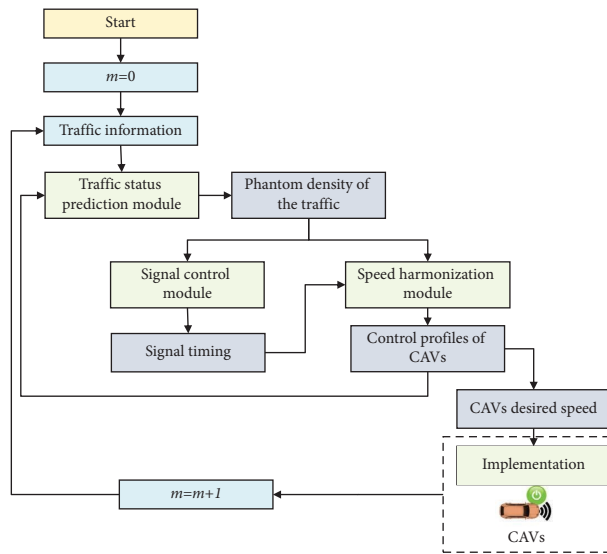


FIGURE 2: Control structure.

lane-changing behaviors. As illustrated in Figure 3, the deceleration of CAVs causes the vehicles behind them to slow down or change lanes. This leads to an increased occupancy rate of road space, even without new vehicles entering. The increased occupancy rate of road space can be imagined as a phantom vehicle increase. This phenomenon is also found in the real world, known as phantom traffic jam [35]. In this situation, speed oscillation results in the occupancy

rate of road space increase. This is equivalent to the phenomenon that density exceeds the critical density, leading to congestion and potential traffic accidents.

To characterize this phenomenon, the concept of phantom density is introduced. It is a formulation developed by this research team [36]. The key takeaways from the previous research are highlighted here. The phantom density is

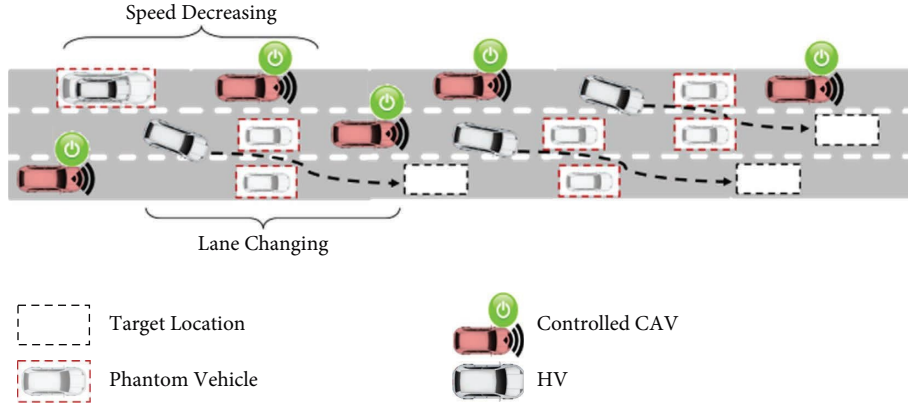


FIGURE 3: The sketch map of the phantom vehicles.

$$\tilde{k}_{m+1}^d = k_m \left[1 + \underbrace{\frac{\gamma_m [v_m - u_{m+1}] \Delta t}{u_{m+1} T}}_{\text{Increase from speed reduction}} + \underbrace{\frac{[v_m - u_{m+1}] (1 - \xi_m) \text{Exp}(-\bar{l} k_m / 1000) t_{LC}}{v_f \Delta t}}_{\text{Increase from additional lane changes}} \right], \quad (1)$$

$$\gamma_m = \begin{cases} 1, & \xi_m > \frac{1}{2}, \\ 2\xi_m, & \xi_m \leq \frac{1}{2}, \end{cases} \quad (2)$$

$$k_m = \frac{\sum_{i=1}^{N_m} t_m^i}{L \Delta t},$$

where \tilde{k}_{m+1}^d is the phantom density when CAVs are decelerating during update time interval +1. γ_m is the portion of vehicles under the influence of CAVs' speed change at update time interval m . ξ_m is the penetration rate of CAVs at update time interval m . When CAVs are more than HVs ($\xi > 1/2$), the movements of all HVs are enforced by CAVs' speed reduction, $\gamma = 1$. Otherwise, only the movements of HVs that are right behind CAVs are influenced, $\gamma = 2\xi$. v_m is the average speed of all vehicles at update time interval m . u_{m+1} is the desired speed of CAVs, the control vector at update time interval $m + 1$. \bar{l} is the average length of vehicles. m is the index of the update time interval. t_{LC} is average lane-changing duration. Δt is the update time interval. T is the length of time that the average speed approaches CAVs' desired speed. N_m is the number of vehicles at update time interval m . t_m^i is the travel time of vehicle i on the control segment at update time interval m . L is the length of control segment.

Note that the density \tilde{k}_{m+1}^d in equation (1) is not actual conventional density. Instead, it is a new concept named phantom density. In terms of phantom density, it refers to the collective summation of both real vehicles and phantom vehicles

traveling at a unit distance. Phantom vehicles are utilized to quantify not only occupancy caused by physical space taken by actual vehicles but also the additional occupancy caused by motions, such as slowing down and lane-changing. When vehicles are slowing down or lane-changing, the same number of vehicles occupies greater space. The greater space occupied is as if there were more vehicles. The derivation and proof of equation (1) have been achieved with a combination of multiple empirical observations and theories. The conservation of vehicles is guaranteed. The related work has been peer-reviewed and published in IEEE Transactions on Intelligent Transportation Systems [36].

(ii) Situation 2: when it is during the green interval.

During the green interval, the change of traffic flow is divided into two stages. The first stage is the early phase of the green signal, where CAVs accelerate to achieve the free-flow speed. The second stage is when CAVs have completed acceleration, and the entire traffic flow reaches the free-flow speed. The entire traffic flow is stable.

The general formulation of the phantom density is as follows:

$$\tilde{k}_{m+1}^a = \begin{cases} k_m \left[1 + \frac{\gamma_m [v_m - u_{m+1}] \Delta t}{u_{m+1} T} \right], u_{m+1} < v_f, \\ k_m, u_{m+1} = v_f, \end{cases} \quad (3)$$

where \tilde{k}_{m+1}^a is the phantom density when CAVs are accelerating during update time interval +1. Note that during this period, the density of traffic gradually decreases. It is similar to the impact of CAVs' speed reduction on density (as equation (1)). However, equation (3) does not take into account the scenario of CAVs' additional lane changes while accelerating. This is because during the red interval, vehicles have already formed a tight traffic flow, and there is no space for lane changes at the beginning of the green interval.

4.4. Signal Control Module. This section provides a detailed introduction to the signal control mechanisms. It includes the signal control flow, signal control strategy, and signal switching criteria.

4.4.1. Signal Control Flow. The signal control module is to calculate the signal timing based on the predicted phantom density. The phantom density is a criterion that determines whether to perform green light extension or phase switching. The working principle of the signal control module is shown in Figure 4.

As shown in the figure, the module first finds the green phase. This is done because the control strategy output by the signal control module relies on density evaluation during the green phase. If there is no green phase at the current time m (indicating a phase switch occurred at time interval $m - 1$), strategy C is executed. If the green phase is found, it is then determined whether a phase switching or an extension of the green time is required. Based on this determination, strategy A or strategy B is executed.

4.4.2. Signal Switching Criteria. In order to ensure the smooth flow of traffic at intersections, signal switching is based on the maximum phase phantom density. The definition of maximum phase phantom density is as follows:

$$\tilde{k}_{\max} = \max \left(\tilde{k}_m^D \right), D = 1, 2, 3, 4, \dots \quad (4)$$

$$\tilde{k}_m^D = \begin{cases} \tilde{k}_{m+1}^a, \text{ state of phase } D = \text{Green}, \\ \tilde{k}_{m+1}^d, \text{ state of phase } D = \text{Red or Yellow}, \end{cases}$$

where \tilde{k}_m^D represents the phantom density of each phase. D represents the number of phases. \tilde{k}_{\max} represents the maximum phase phantom density. It serves as a critical parameter in determining the signal switching strategy.

The signal is switched when the maximum phase phantom density is arrived at a threshold. Since the signal switching is mainly about green light extension or phase switching, the switching criteria are focused on the density during the green interval. The proposed strategy gives priority to releasing phases with high phantom density. However, these phase switching criteria sometimes result in a waste of effective green time. To address this issue, a switching threshold, denoted as k_M , has been introduced in the strategy. The purpose of this threshold is to ensure the efficiency of the entire traffic when a phase switch occurs. It is achieved by introducing a buffer density.

$$k_{m_b}^D = \begin{cases} \tilde{k}_m - \tilde{k}_{(m-G_{\min}/\Delta t)}, T_m^R = G_{\min}, \\ k_{m_b}^D, \text{ else,} \end{cases} \quad (5)$$

$$\tilde{k}_{\max} \leq k_{m_b}^D + k_m^G, \quad (6)$$

where $k_{m_b}^D$ is the buffer density for phase switching of the D phase at time interval m . T_m^R indicates the duration of the red interval during update time interval m . G_{\min} represents the minimum green time. The update of buffer density $k_{m_b}^D$ is triggered when the duration of the red interval T_m^R equals G_{\min} . This value represents the density variation of the current phase within the minimum green time since the last switch from green to red.

Note that equation (5) ensures that the switching thresholds for each phase are different and constantly updated. Therefore, this ensures the adaptation of the switching thresholds to various traffic conditions.

Equation (6) ensures that the increase in density does not exceed the density difference between the green phase and the current red phase. The conditions for triggering a phase switch will not be met again within the G_{\min} time.

In order to avoid phantom congestion in controlled sections, there should be

$$\tilde{k}_{\max} \leq \min \left(k_{m_b}^D + k_m^G, k_C \right), \quad (7)$$

where k_C represents the critical density of the control segment. k_m^G is the density of the green phase at time interval m .

Before deciding on the signal control strategy for the next time window, it is also necessary to ensure that the green interval duration meets

$$T_m^G \in [G_{\min}, G_{\max}], \quad (8)$$

where G_{\min} represents the minimum green time. G_{\max} represents the maximum green time.

4.4.3. Signal Control Strategy. Considering the potential situations like green interval extension and phase switch, three strategies are proposed. Strategies A and B are set at the green phase. Strategy C addresses the situation of the yellow signal phase (when none of the phases are green). This design simplifies the execution of signal timing for each phase. Details are as follows.

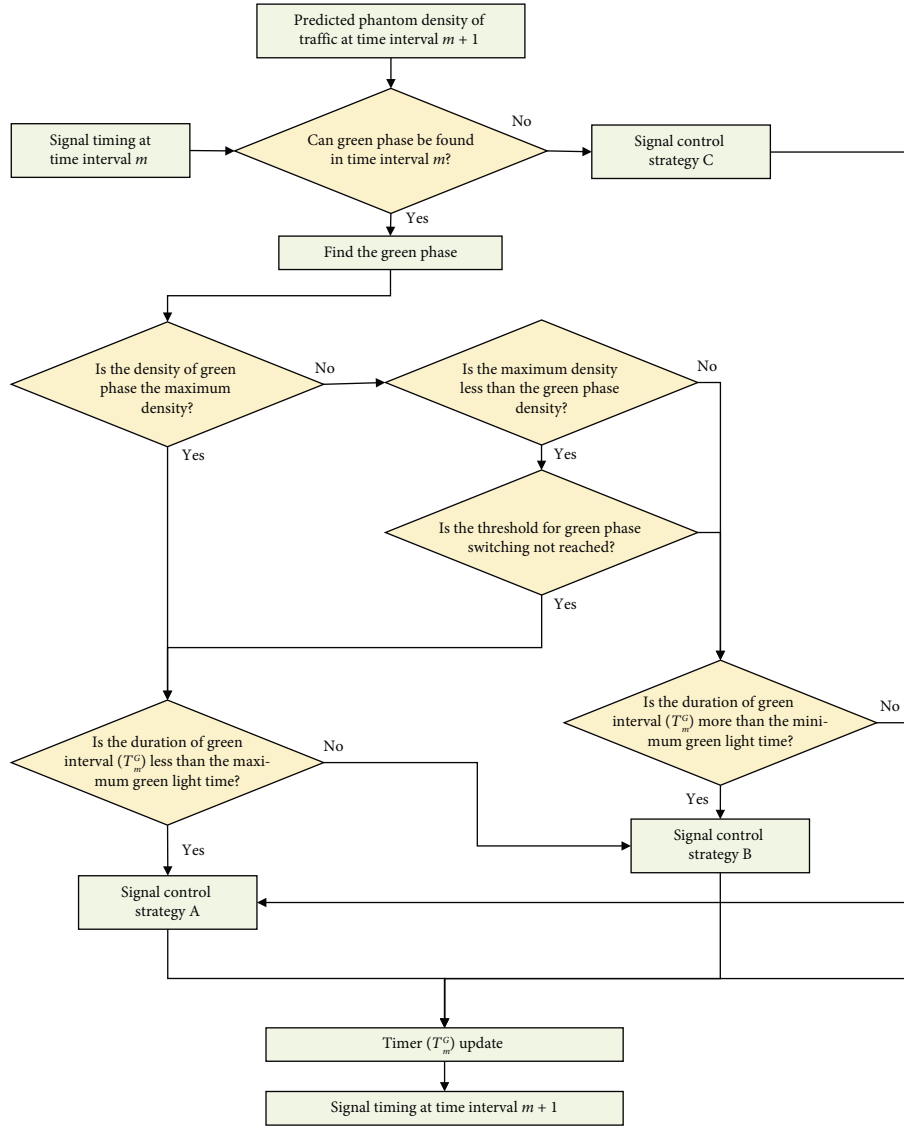


FIGURE 4: Signal control module.

(i) Signal control strategy A

Strategy description: The green signal phase will remain green in the next time window. The other signal phases will remain red.

Activated conditions: if equation (7) is satisfied.

(ii) Signal control strategy B

Strategy description: the green signal phase will change to yellow in the next time window, while the other signal phases will remain green.

Activated conditions: if equation (7) is not satisfied.

(iii) Signal control strategy C

Strategy description: in the next time window, the signal phase with the maximum density will be changed to green, while the other signal phases will be changed to red.

Activated conditions: if there is no green phase at the current time m .

Note that in strategy C, there is currently no green signal phase. This means that strategy B was executed in the previous time window.

To facilitate its operations, the module utilizes a timer T_m^G , which records the duration of the current green interval. Every time the signal control module is activated, the timer is incremented by Δt after the output is generated. When the phase changes to red, the timer is reset to zero and begins timing again. According to different strategies, the changes in the timer can be represented as follows:

$$T_m^G = \begin{cases} T_m^G + \Delta t, & \text{strategy A or strategy B,} \\ 0, & \text{strategy C.} \end{cases} \quad (9)$$

4.5. *CAV Speed Harmonization Module.* This section presents the details of the CAV speed harmonization module. It includes the workflow of speed harmonization and CAV speed harmonization strategy.

The Workflow of CAV Speed Harmonization. The workflow of the CAV speed harmonization module is shown in Figure 5. CAV speed harmonization module takes the signal timing information for update time interval $m + 1$ as input and generates the desired speed for CAVs at update time intervals $(m + 1)$ and $(m + 2)$ as output. In order to achieve this, it is necessary to predict the desired speed of CAVs at $m + 1$. However, due to computational constraints, the strategy employed for $m + 1$ will be extended to $m + 2$ for predicting the desired speed.

In this paper, the speed harmonization strategy for CAVs is determined based on the signal strategy. It enables the coordination between the CAV speed harmonization strategy and signal control strategy. Based on the input of signal timing, the situation for CAV speed harmonization is divided into four scenarios, as shown in Figure 6.

As shown in the figure, situation division for CAV speed harmonization consists of four scenarios: (1) green to green, (2) red to red, (3) green to yellow and yellow to red, and (4) red to green. Note that scenario 3 covers two cases. The switching from green to yellow and subsequently to red represents a continuous change. Hence, the corresponding speed harmonization strategy remains consistent.

CAV Speed Harmonization Strategy. CAV speed harmonization strategy is proposed to adapt to the signal control situations. The detailed strategies for various situations are as follows.

4.5.1. Speed Harmonization Strategy 1. Activated condition: where the current phase and the next phase are green.

In this situation, the controller is influenced by the queue state at the intersection. If there are queued vehicles ahead, the premature acceleration of vehicles may result in an increase in the average number of stops. Therefore, the controller will output acceleration commands only after the queued vehicles have dispersed. If there are no queued vehicles ahead, CAVs will begin accelerating until they reach the speed limit on the road. This helps to achieve maximum throughput while maintaining efficiency. The strategy is outlined as follows:

$$v_{m+1}^D = \begin{cases} v_m^D, T_m^G \leq t_s, \\ v_m^D + a_{\max} \Delta t, T_m^G > t_s \text{ and } v_m^D \leq v_{rl}, \\ v_{rl}, v_m^D = v_{rl}, \end{cases} \quad (10)$$

where v_m^D represents the desired speed of CAVs in phase D during update time interval m . v_{rl} represents the road limit speed. t_s represents the start-up time of the last vehicle in the queue.

If the queue exists, it is necessary to determine the time when the last vehicle started. We assume that the relationship between traffic flow and density follows the triangular fundamental diagram [37]. The triangular fundamental diagram adopted is shown in Figure 7.

When the upstream density is greater than the downstream density, the dissipation speed of the rarefaction wave can be represented as $-w$. It is calculated as follows:

$$w = \frac{q_c}{k_{\text{jam}} - k_c}. \quad (11)$$

Since vehicles are queued at the intersection during the red interval, the queue flow is with congested density k_j . When the green interval begins, the first vehicle starts accelerating, and the rarefaction wave begins propagating backward at a speed of w [38]. When the rarefaction wave reaches the last queued vehicle, all queued vehicles have completed their start-up behavior. The analysis of the rarefaction wave provides a theoretical basis for estimating the vehicle start-up time. The estimation of the time t_s when the last vehicle in the queue starts can be expressed as follows:

$$t_s = \frac{N_q(\bar{l} + \bar{h}_s)}{w}, \quad (12)$$

where t_s represents the start-up time of the last vehicle in the queue, N_q represents the number of queued vehicles in the current lane, \bar{h}_s represents the average stopping distance of vehicles when queuing, and \bar{l} is the average length of vehicles.

4.5.2. Speed Harmonization Strategy 2. Activated condition: where the current phase and the next phase are red.

In this situation, CAVs would slow down and form a tight queue of traffic flow. The speed is calculated as follows:

$$v_{m+1}^D = v_m^D + \Delta v_{m_{\max}}^D \Delta t, \quad (13)$$

where $\Delta v_{m_{\max}}^D$ is the maximum speed change that satisfies equation (21) (defined on page 18).

To avoid collision risks created by the preceding CAVs decelerating, it is necessary to impose limitations on the behavior of CAVs' deceleration. The minimum following distance of a vehicle is composed of three parts: the length of the preceding vehicle, the safety buffer zone, and the driver reaction time gap, as shown in Figure 8.

The calculation of relevant parameters is as follows:

$$S_{\min} = \tau(v_b - v_a) + \Delta_{\text{safe}} + \bar{l}, \quad (14)$$

$$\Delta_{\text{safe}} = v_m^D H_s, \quad (15)$$

where S_{\min} is the shortest following distance, τ is the driver's response time, usually taken between 0.3 s and 2 s, v_a is the speed of the preceding vehicle, v_b is the speed of the following car, Δ_{safe} is the safety buffer, v_m^D is the average speed of the vehicles in phase D during update time interval m , and H_s is safe time headway.

In the context of this scenario, we assume that the preceding and following vehicles are moving at the same speed before CAVs conduct decelerating. In this case, the average speed change can be expressed as

$$\Delta v_m^D = \frac{v_a - v_b}{\Delta t}. \quad (16)$$

Based on the phantom density, we can obtain the average headway distance during time interval m of phase D , denoted as \bar{S}_m^D . For safety considerations, we should have

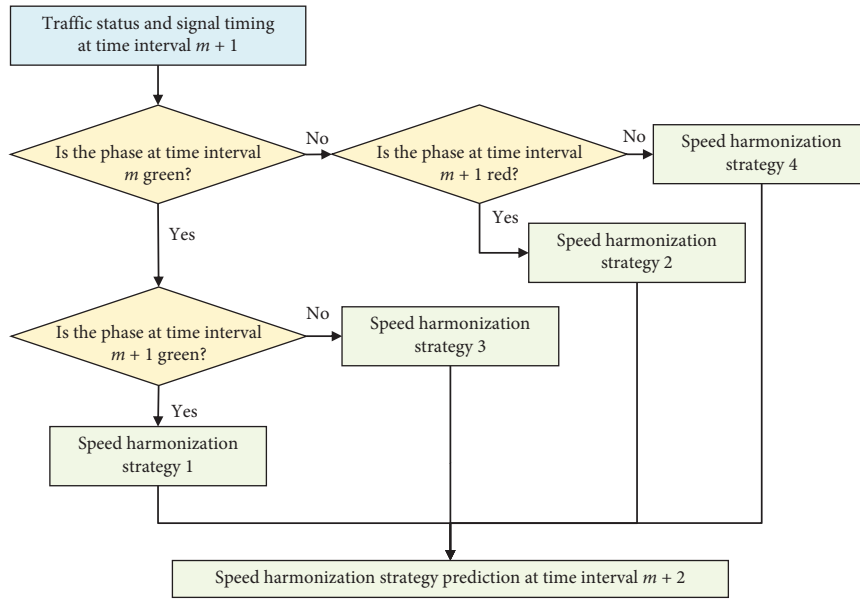


FIGURE 5: CAV speed harmonization module.

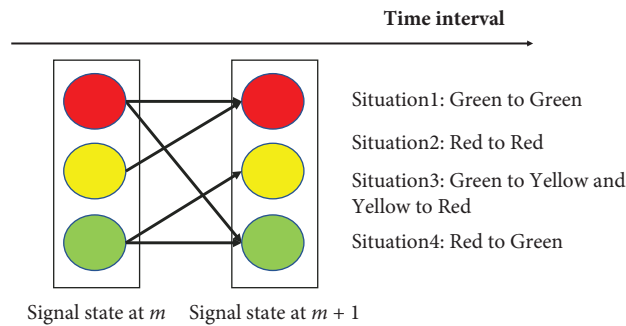


FIGURE 6: Situation division for CAV speed harmonization.

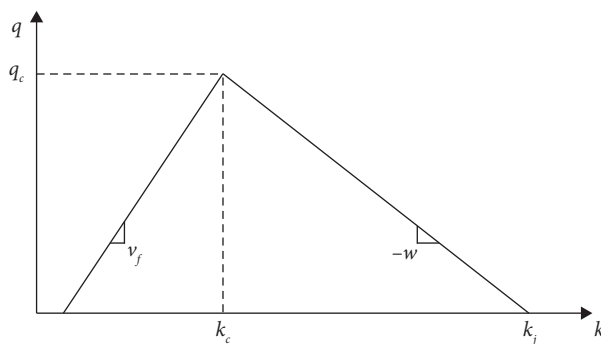


FIGURE 7: The triangular fundamental diagram.

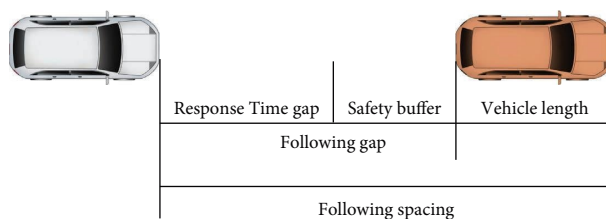


FIGURE 8: Illustration of the following spacing.

$$\tilde{S}_m^D = \frac{1}{\tilde{k}_m^D}, \quad (17)$$

$$\tilde{S}_m^D - S_{\min} \geq 0. \quad (18)$$

According to equations (16)–(20), we can obtain

$$\Delta v_m^D \geq \frac{\tilde{k}_m^D (v_m^D H_s - \bar{l}) - 1}{\tilde{k}_m^D \tau \Delta t}. \quad (19)$$

The deceleration of CAVs requires the constraint of speed variation and safety. The constraint is as follows:

$$\Delta v_m^D \in [a_{\min}, a_{\max}], \quad (20)$$

where Δv_m^D represents phase D during update time interval m . a_{\min} and a_{\max} are the thresholds for changes in speed. These thresholds are designed to prevent CAVs from being unable to effectively execute the desired speed.

According to safety constraints and speed change constraints, the maximum value of speed change can be obtained as follows.

Combining equations (19) and (20), the maximum value of speed change can be obtained as

$$\Delta v_{m_max}^D = \max \left(\frac{\tilde{k}_m^D (v_m^D H_s - \bar{l}) - 1}{\tilde{k}_m^D \tau \Delta t}, a_{\min} \right). \quad (21)$$

4.5.3. Speed Harmonization Strategy 3. Activated condition: where the current phase is green, but the next phase would switch to yellow.

In this situation, CAVs start decelerating from the state of driving at the maximum speed limit. Similar to strategy 2, the desired speed for CAVs in the next time window is

$$v_{m+1}^D = v_m^D + \Delta v_{m_max}^D \Delta t. \quad (22)$$

4.5.4. Speed Harmonization Strategy 4. Activated condition: where the current phase is red, but the next phase will switch to green.

In this situation, the strategy should consider the time for vehicles' start-up. It needs to predict the start-up time of the trailing vehicle and deliver acceleration commands to the CAVs after its start-up. The calculation of the start-up time t_s for the trailing vehicle is given by equation (12).

Similar to strategy 1, once the last queued vehicle completes its start-up, the CAVs in the traffic flow would receive acceleration instructions. The desired speed for CAVs is calculated as

$$v_{m+1}^D = \begin{cases} v_m^D, T_m^G \leq t_s, \\ v_m^D + a_{\max} \Delta t, T_m^G > t_s \text{ and } v_m^D \leq v_{rl}, \\ v_{rl}, v_m^D = v_{rl}. \end{cases} \quad (23)$$

5. Evaluation

This section evaluates the proposed strategy through microscopic simulation. This section presents the simulation platform, experimental design, and results. The experimental design includes test scenarios, compared baseline, sensitivity analysis design, measurement of effectiveness (MOE), and result analysis.

5.1. Simulation Platform. The validation of the proposed strategy is conducted on a simulation platform developed by this research team. The platform is based on VISSIM but has been enhanced explicitly for a partially connected and automated traffic environment. The driving model of CHVs adopted is VISSIM internal model and calibrated using naturalistic driving data collected from Shanghai. The movement of CAVs is controlled by a commercialized controller which is developed for China's Original Equipment Manufacturer (OEM) Shanghai Automotive Industry Corporation (SAIC) by this research team.

Trajectories of the simulated CAVs are validated with results of California Partners for Advanced Transportation Technology (PATH) from their field experiment in terms of speed, acceleration, and time gap. Hence, the simulation platform has been validated with the capability of replicating the traffic with a mixture of advanced driver-assistance system- (ADAS-) equipped vehicles. The work has been peer-reviewed and published in Transportation Research Part C [39].

Note that to simulate the phenomenon that CAVs cannot change to the speed delivered by the control center instantly, the speed command passed to the simulation platform is the desired speed of CAVs. The actual speed of CAVs is calculated by the vehicle actuator.

5.2. Experiment Design

5.2.1. Testbed. The testbed of the simulation experiment is constructed based on a real intersection. The intersection is located in Yizhang, Beijing. The structure of the studied intersection is shown in Figure 9. The signal timing of the intersection is shown in Figure 9(c).

5.2.2. Tested Scenarios. Three scenarios considering various compositions of vehicles and signal control schemes are tested:

- (i) *Non-control (base)*: In this scenario, there is no optimization of vehicles' speed and signal control schemes. All vehicles are CHVs. There is no speed advice for CHVs. The signal control scheme operates on fixed predetermined signal timings. It is a base to illustrate the necessity of optimization.
- (ii) *State-of-the-art strategy*: In this scenario, general traffic is composed of CAVs and CHVs. The signal controller and vehicles can transmit information, which allows intersections to optimize signal timing

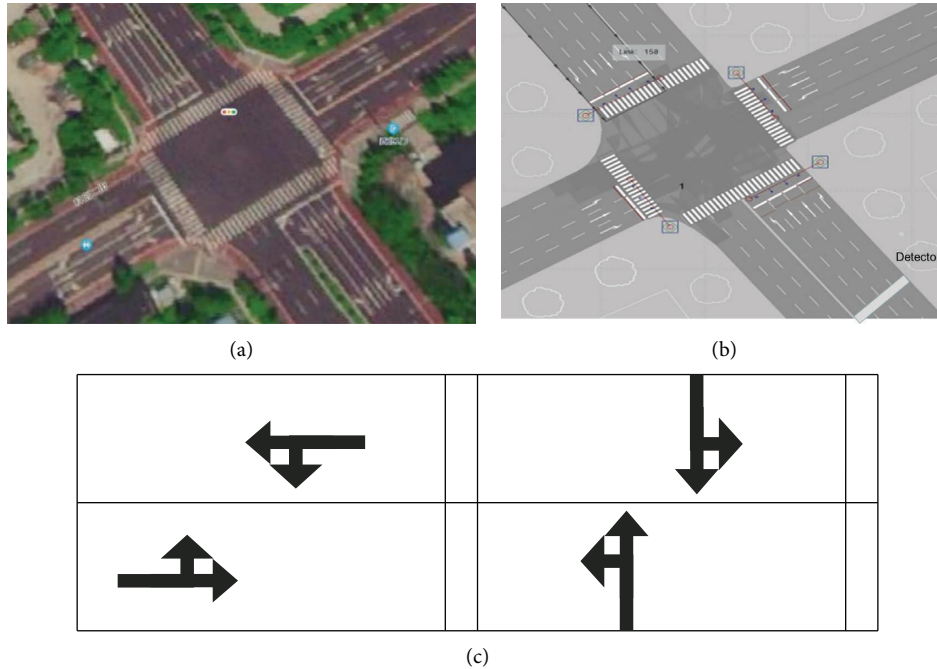


FIGURE 9: The studied scenario: (a) bird view of the intersection, (b) intersection built in simulation, and (c) initial signal phase information.

TABLE 2: Simulation settings.

Parameter	Value
Length of the segment under control (m)	500
Distance from loop detector to stop line	600
Simulation duration (s)	1200
The update time interval of signal control (s)	3
Duration of initial red light (s)	30
Duration of initial green light (s)	30
Duration of yellow light (s)	3
Minimum green time interval (s)	15
Maximum green time interval (s)	45
Saturation flow rate (veh/h)	1440
Maximum acceleration (m/s^2)	3.5
Minimum acceleration (m/s^2)	-4
Safe time headway (s)	1.6
Reaction time (s)	0.5
Free-flow speed (km/h)	40
Jam distance (m)	5
The average length of vehicles (m)	4.5
The update time interval of CAVs' control	1
The gradient of the road segment	0
Safe following distance (m)	1.2

based on the arrival of vehicles. The signal timing optimization method adopted refers to a real-time adaptive traffic control algorithm by utilizing data from connected vehicles [40].

- (iii) *The proposed strategy*: In this scenario, general traffic is composed of CAVs and CHVs. All CAVs are controlled by the proposed speed harmonization controller.

Note that the state-of-the-art strategy selected is based on their feasibility for near-future implementation. The real-time adaptive signal control strategy is currently advanced

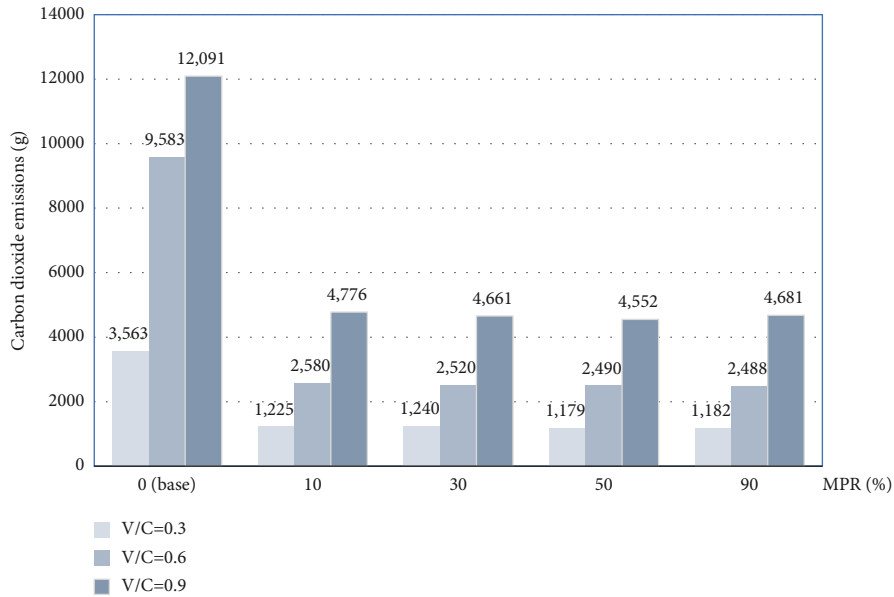
technology that has been successfully applied in real-world intersections, making them a suitable reference method. Furthermore, the real-time adaptive control only adjusts the right of way, while the proposed strategy in this paper regulates both the right of way and traffic demand. This contrast between the two approaches provides an effective comparison.

5.2.3. Simulation Settings. The parameter settings in the simulation experiment are shown in Table 2.

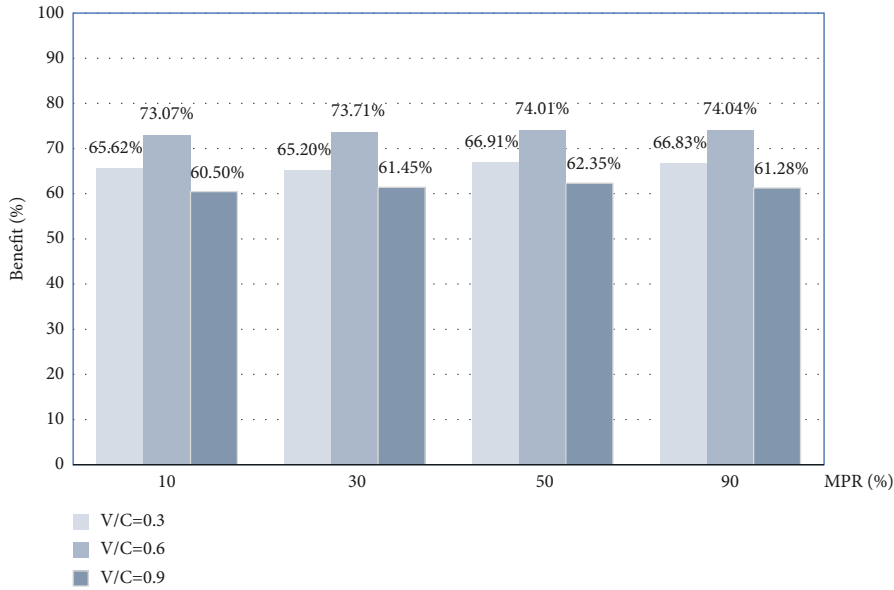
5.2.4. Sensitivity Analysis. Sensitivity analysis of control methods is conducted for different demand levels and MPRs of CAVs. The demand level is quantified by the V/C ratio (volume to capacity ratio). The demand level varies from 0.3 to 0.9 by a 0.3 interval. It represents the low, medium, and high demand levels. The MPR of CAVs is set as 10%, 30%, 50%, and 90%.

5.2.5. Measurement of Effectiveness. To investigate the effectiveness of the proposed strategy, three measurements of effectiveness (MOEs) are adopted, including CO₂ emission, stop frequency, and throughput. They are utilized to quantify the performance of the proposed strategy in terms of ecology and mobility.

CO₂ emission and the vehicle stop frequency are utilized to measure the improvement of ecology environment. CO₂ emission is calculated using the VSP model [41, 42]. The vehicle stop frequency is defined as the average number of stops of all vehicles. It is also utilized to prove the rationale behind the control mechanism (refer to Section 2). The benefit brought by the proposed controller is the reduction of stops.



(a)



(b)

FIGURE 10: CO₂ emissions (g) and benefits (%) compared with the non-control baseline. (a) Average CO₂ emissions (g). (b) CO₂ emission benefits (%).

Throughput is utilized to measure mobility improvement. It is defined as the total number of vehicles passing through the intersection during the entire control duration.

5.3. Results. This section presents the simulation results. Results are averaged from 1200 sets of simulations, including different demand levels and MPRs. Considering the randomness of traffic flow, each group of simulations has 10 random seeds.

Results confirmed that the proposed strategy can reduce emissions while maintaining throughput. The advantages of the proposed strategy can be observed in emission reduction, throughput improvement, and reduction in average stop frequency.

Compared to the non-control base, the proposed approach can achieve a reduction in emissions ranging from 60.50% to 74.04%, an increase in throughput of at least 2.96%, and a decrease in the stop frequency up to 85.82%.

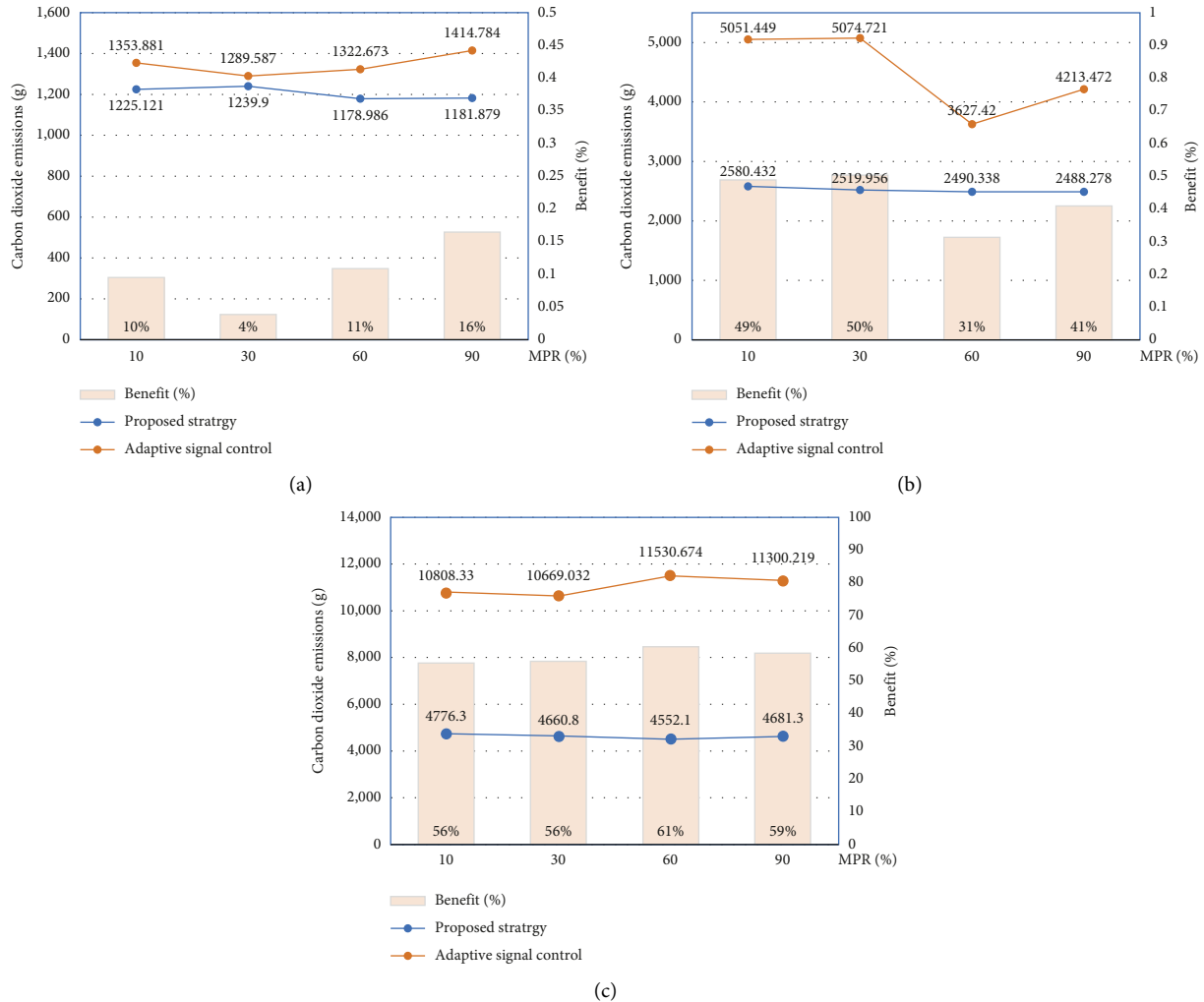


FIGURE 11: Average CO₂ emissions (g) and benefits (%) compared with the state-of-the-art strategy. (a) V/C = 0.3. (b) V/C = 0.6. (c) V/C = 0.9.

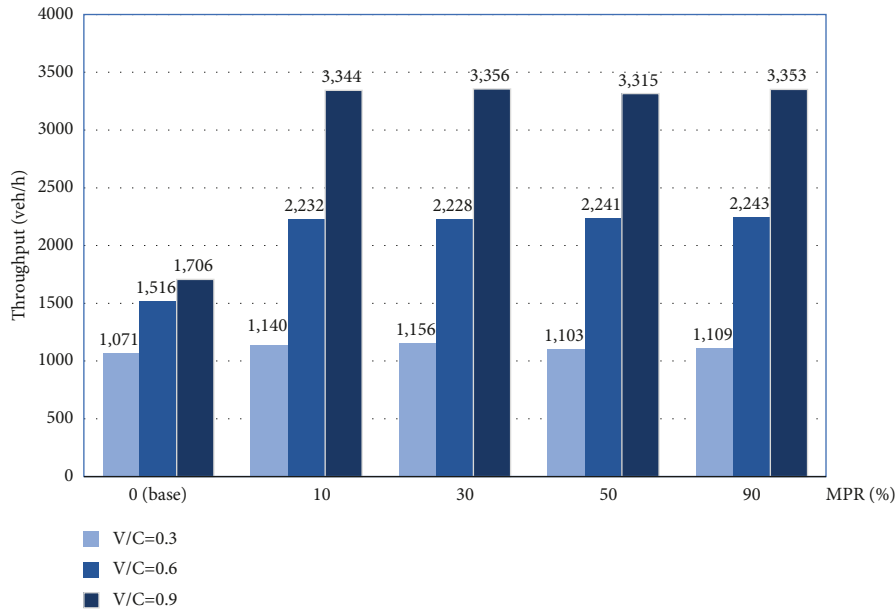
Compared to the state-of-the-art strategy, the proposed approach can achieve a reduction in emissions ranging from 4% to 61%, an average increase in throughput of around 14.91%, and a decrease in the stop frequency ranging from 26% to 81%. It performs better at high demand levels. When V/C = 0.9, the strategy achieves a reduction in emissions ranging from 56% to 61% and an increase in throughput ranging from 37% to 46%. Additionally, it reduces the number of stops by 78% to 81%.

5.3.1. CO₂ Emissions

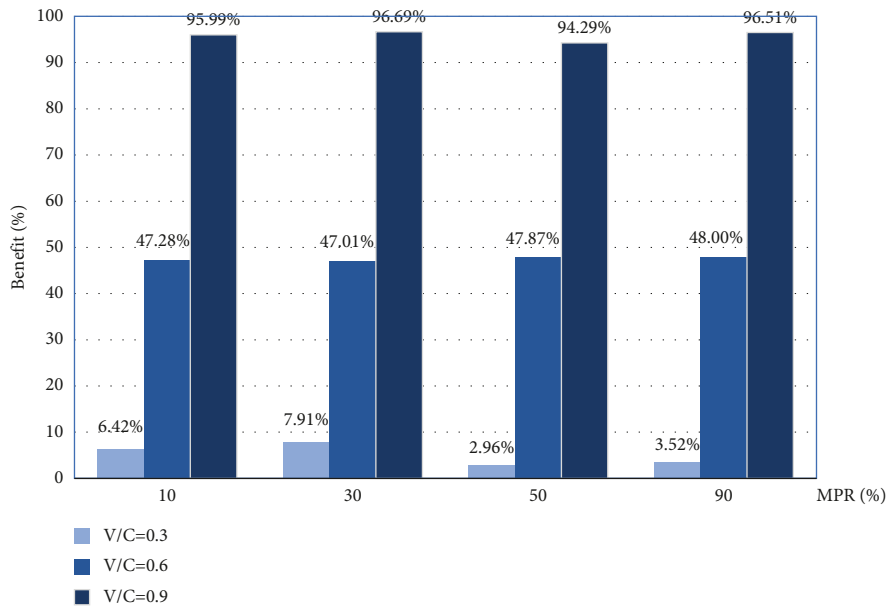
(1) *Comparison against Non-Control Baseline.* Figure 10 shows CO₂ emissions and benefits under various demand levels and MPRs of CAVs. The proposed strategy demonstrates significant benefits at similar demand levels, with minimal fluctuations in benefits across different MPRs of CAVs. It can achieve a reduction in emissions ranging from 60.50% to 74.04%. This indicates that the method overcomes the existing system’s dependence on high penetration rates of CAVs. Under the same MPR, the

method achieves maximum benefits at the middle demand level (V/C = 0.6). This is because, at lower demand levels, the number of vehicles affected by CAVs’ deceleration is limited, resulting in some CHVs waiting at intersections. However, the proposed strategy at higher demand levels aims to prevent traffic congestion during red intervals, leading to a reduction in CAVs’ deceleration behavior. This sacrifice in optimization performance is made to ensure traffic flow stability.

(2) *Compared with State-of-the-Art Strategy.* Figure 11 shows the comparison between the proposed strategy and state-of-the-art strategy in CO₂ emissions. Compared to the state-of-the-art strategy, the proposed strategy can reduce emissions by 31% to 61% under medium to high demand levels (V/C = 0.6 and V/C = 0.9), and the performance is superior to the existing studies (10%~41%) [25, 43]. At low demand levels (V/C = 0.3), the strategy can reduce CO₂ emissions by 4% to 16%, with fewer benefits compared to high demand levels. This is because, in low demand levels, fewer vehicles need to stop and wait, resulting in limited optimization benefits.



(a)



(b)

FIGURE 12: The throughput (veh/h) and benefits (%) compared with the non-control baseline. (a) Average throughput (veh/h). (b) Throughput benefits (%).

5.3.2. Mobility

(1) *Comparison against the Non-Control Baseline.* Figure 12 shows the average throughput benefits under various demand levels and MPRs of CAVs. The proposed strategy can achieve an improvement in throughput ranging from 2.96% to 96.69%. The proposed strategy is beneficial across different demand levels. As demand levels increase, the benefits of the strategies also increase gradually. The strategies proposed at moderate demand levels and high demand levels (V/C = 0.6 and V/C = 0.9) demonstrate consistent performance across various MPRs of CAVs. Additionally, this

demonstrates that the method can ensure throughput at intersections while reducing emissions.

(2) *Compared with State-of-the-Art Strategy.* Figure 13 shows the comparison between the proposed strategy and the state-of-the-art strategy in average throughput. Compared to the state-of-the-art strategy, the proposed strategy can improve average throughput by around 14.91%. In low demand levels, the effectiveness of both methods is nearly the same. As demand levels increase, the advantages of the proposed strategies gradually become more pronounced. At high demand levels, the throughput is increased by 36% to 46%

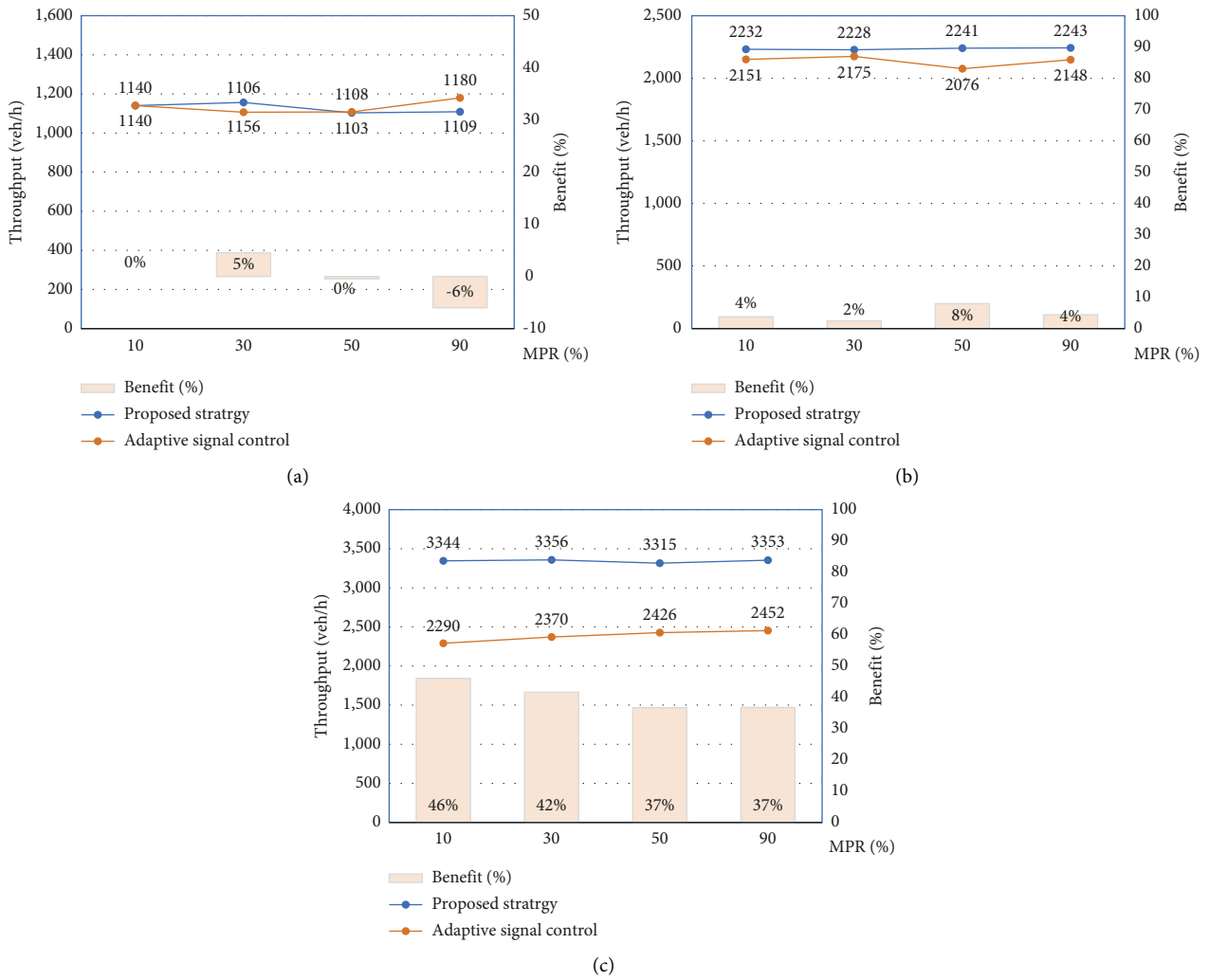
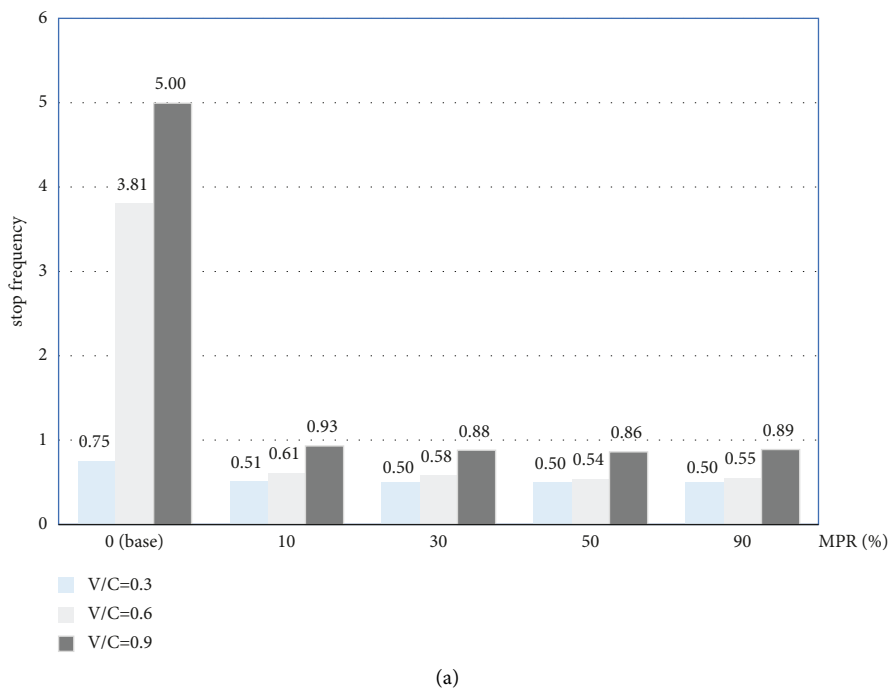


FIGURE 13: Average throughput (veh/h) and benefits (%) compared with the state-of-the-art strategy. (a) V/C = 0.3. (b) V/C = 0.6. (c) V/C = 0.9.



(a) FIGURE 14: Continued.

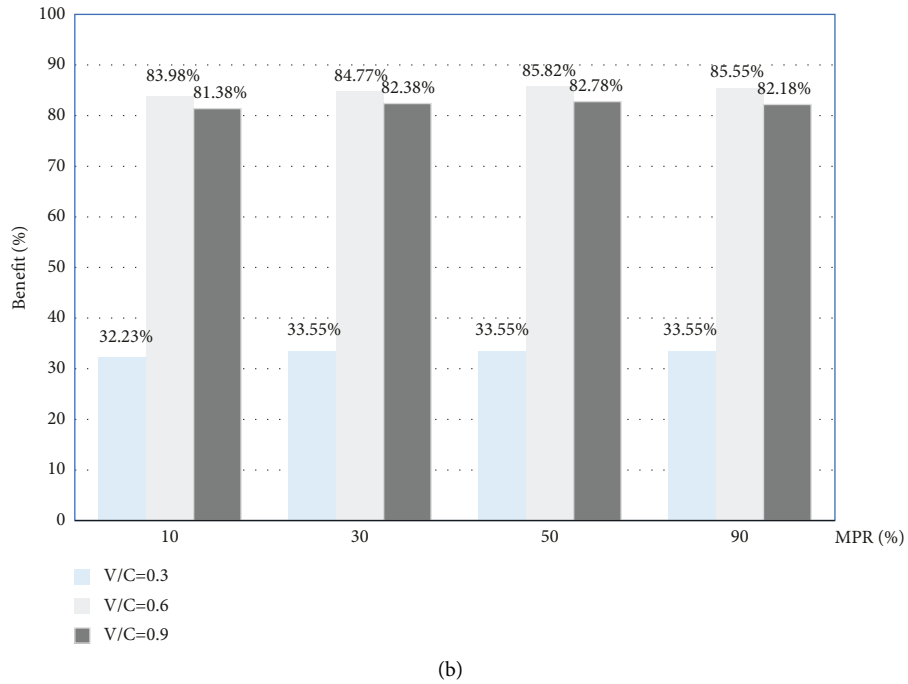


FIGURE 14: Stop frequency and benefits (%) compared with the non-control baseline. (a) Average stop frequency. (b) Stop frequency benefits (%).

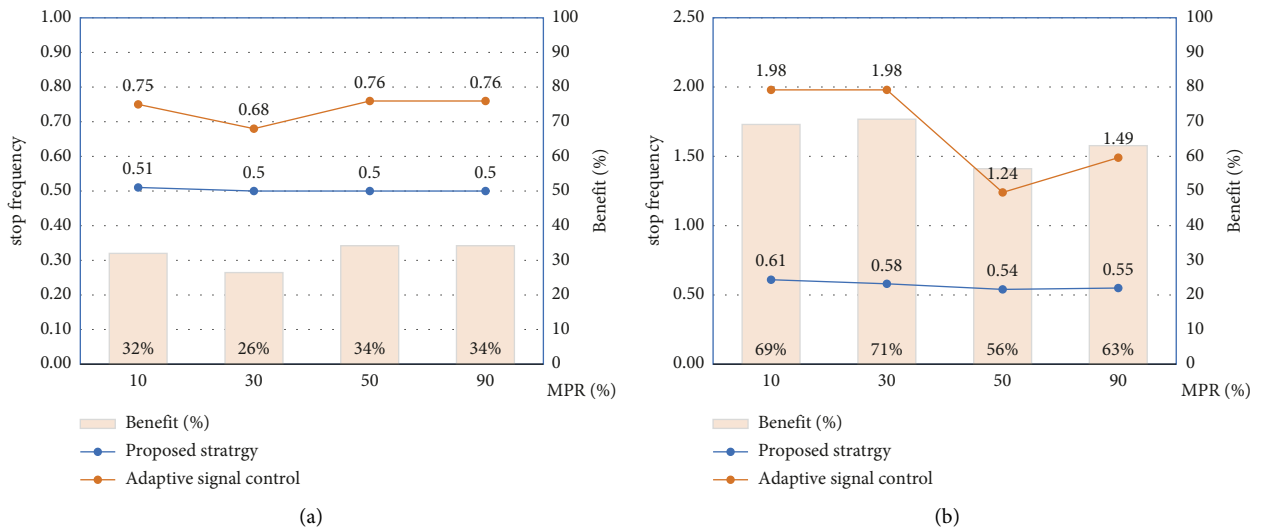


FIGURE 15: Continued.

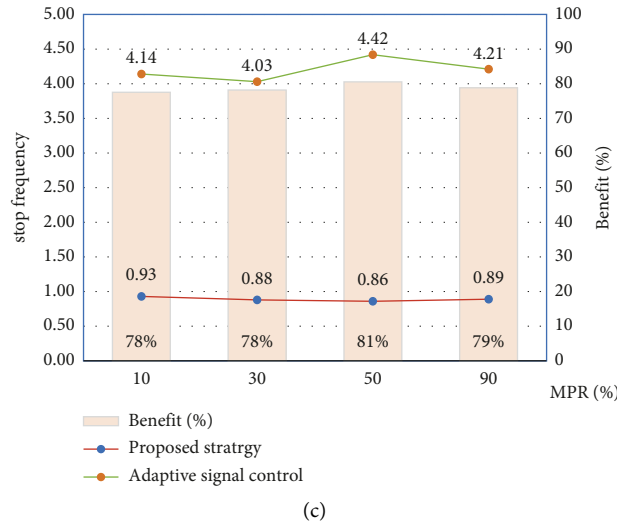


FIGURE 15: Average stop frequency and benefits (%) compared with the state-of-the-art strategy. (a) $V/C = 0.3$. (b) $V/C = 0.6$. (c) $V/C = 0.9$.

compared to the state-of-the-art strategy method. This makes sense because non-congested roads can easily handle all vehicles, so there is little room for throughput improvement.

5.3.3. The Vehicle Stop Frequency

(1) *Comparison against the Non-Control Baseline.* Figure 14 shows the stop frequency benefits under various demand levels and MPRs of CAVs. The proposed strategy can achieve a reduction in stop frequency ranging from 32.23% to 85.82%. The proposed strategy demonstrates significant advantages in reducing stop frequency across various demand levels. The average stop frequency ranges between 0.51 and 0.61 in low congestion and moderate demand levels, which validates the effectiveness of the approach. In moderate and high demand levels, the average parking frequency benefits is reduced by at least 81%. The proposed strategy shows no significant fluctuations across different MPRs of CAVs, thereby proving the feasibility of controlling the traffic flow through a small number of CAVs. It is worth mentioning that the average stop frequency of the proposed strategy is less than 1, which means most vehicles are able to travel through the intersection without stopping.

(2) *Compared with State-of-the-Art Strategy.* Figure 15 shows the comparison between the proposed strategy and the state-of-the-art strategy in average stop frequency. Compared to the state-of-the-art strategy, the proposed strategy can reduce stop frequency from 26% to 81%. The reason for the significant optimization results is that the proposed strategy coordinates signal timing with CAVs' speed harmonization. As the saturation levels increase, the advantages of this method become more pronounced. When $V/C = 0.9$, the benefits of the strategy reach 78% to 81%. The strategy's performance remains stable across different MPRs of CAVs. By combining the analysis in Sections 5.3.1 and 5.3.2, it can

be observed that the main reason for the improvement in traffic efficiency and emission reduction lies in the significant reduction in stop frequency. Since the start-stop behavior of vehicles is closely related to intersection efficiency and emissions, reducing the number of parking instances improves the effective utilization of green lights at intersections and directly reduces additional greenhouse gas emissions.

6. Conclusions and Future Research

This study proposes an eco-speed harmonization method for partially connected and automated traffic. The strategy is able to achieve emission reduction and improve mobility under different traffic conditions. It also has potential implementations in the near future (at the early stage where CAVs' MPR is low). To evaluate the proposed controller, a VISSIM-based microscopic simulation evaluation was conducted. Sensitivity analysis was performed for CAV MPR and demand level (V/C ratio). The evaluation shows the following:

- (i) The proposed approach can achieve a reduction in emissions ranging from 4% to 61%, an average increase in throughput of around 14.91%, and a decrease in the stop frequency ranging from 26% to 81%.
- (ii) Under various MPRs of CAVs, the proposed strategy demonstrates stable optimization effects. No significant fluctuations in the optimization effects have been observed with changes in MPR. This indicates the advantages of controlling the entire connected and automated traffic as a whole.
- (iii) Under different demand levels, the benefits of the proposed strategy increase as the demand level rises. It means that the proposed strategy performs better at a high demand level. When $V/C = 0.9$, compared to the state-of-the-art strategy, the proposed strategy achieves a reduction in emissions ranging from

56% to 61%, an increase in throughput ranging from 37% to 46%, and a decrease in the stop frequency ranging from 78% to 81%.

- (iv) Under varying MPRs and demand levels, the proposed strategy consistently demonstrates a superior performance regarding the average number of stops, which is consistently below 1. This indicates that the majority of vehicles can pass through the intersection without having to stop.

It is worth noting that the proposed method is a general eco-approach for controlling partially connected and automated traffic at intersections. It can be extended to dynamic green wave scenarios. In future research, the coordination of signals across multiple intersections could be considered, potentially leading to further reductions in traffic emissions. Furthermore, drawing inspiration from existing methods for eco-driving with CAVs, incorporating varying recommended speeds based on vehicle positions within the traffic flow could be explored, potentially aiding in the enhancement of the method.

Data Availability

No data were used to support this study.

Conflicts of Interest

The authors declare that there are no conflicts of interest regarding the publication of this paper.

Acknowledgments

This study was partially supported by the National Natural Science Foundation of China (grant no. 52072264).

References

- [1] I. E. Agency, *CO2 Emissions from Fuel Combustion*, International Energy Agency, Paris, France, 2018.
- [2] K. Brookhuis and D. de Waard, "Limiting speed, towards an intelligent speed adapter (ISA)," *Transportation Research Part F: Traffic Psychology and Behaviour*, vol. 2, no. 2, pp. 81–90, 1999.
- [3] K. Katsaros, R. Kernchen, M. Dianati, and D. Rieck, "Performance study of a Green Light Optimized Speed Advisory (GLOSA) application using an integrated cooperative ITS simulation platform," in *Proceedings of the 7th International Wireless Communications and Mobile Computing Conference, IWCMC*, Istanbul, Turkey, July 2011.
- [4] H. Xia, K. Boriboonsomsin, and M. Barth, "Dynamic eco-driving for signalized arterial corridors and its indirect network-wide energy/emissions benefits," *Journal of Intelligent Transportation Systems*, vol. 17, no. 1, pp. 31–41, 2013.
- [5] M. Barth and K. Boriboonsomsin, "Energy and emissions impacts of a freeway-based dynamic eco-driving system," *Transportation Research Part D: Transport and Environment*, vol. 14, no. 6, pp. 400–410, 2009.
- [6] Y. Luo, S. Li, S. Zhang, Z. Qin, and K. Li, "Green light optimal speed advisory for hybrid electric vehicles," *Mechanical Systems and Signal Processing*, vol. 12, 2016.
- [7] S. Yu, R. Fu, Y. Guo, Q. Xin, and Z. Shi, "Consensus and optimal speed advisory model for mixed traffic at an isolated signalized intersection," *Physica A: Statistical Mechanics and Its Applications*, vol. 531, Article ID 121789, 2019.
- [8] W. H. Lee and J. Y. Li, "An eco-driving advisory system for continuous signalized intersections by vehicular ad hoc network," *Journal of Advanced Transportation*, vol. 2018, Article ID 5060481, 12 pages, 2018.
- [9] J. Zhao and W. Ma, "An alternative design for the intersections with limited traffic lanes and queuing space," *IEEE Transactions on Intelligent Transportation Systems*, vol. 22, no. 3, pp. 1473–1483, 2021.
- [10] Y. Shao and Z. Sun, "Eco-approach with traffic prediction and experimental validation for connected and autonomous vehicles," *IEEE Transactions on Intelligent Transportation Systems*, vol. 99, pp. 1–11, 2020.
- [11] V. Ardalan and S. Antonio, "Energy saving potentials of connected and automated vehicles," *Transportation Research Part C Emerging Technologies*, vol. 20, 2018.
- [12] N. Goulet and B. Ayalew, "Distributed maneuver planning with connected and automated vehicles for boosting traffic efficiency," *IEEE Transactions on Intelligent Transportation Systems*, vol. 99, pp. 1–15, 2021.
- [13] Y. Feng, C. Yu, and H. X. Liu, "Spatiotemporal intersection control in a connected and automated vehicle environment," *Transportation Research Part C: Emerging Technologies*, vol. 89, pp. 364–383, 2018.
- [14] A. Danesh, W. Ma, C. Yu, R. Hao, and X. Ma, "Optimal roundabout control under fully connected and automated vehicle environment," *IET Intelligent Transport Systems*, vol. 15, no. 11, pp. 1440–1453, 2021.
- [15] P. Chen, C. Yan, J. Sun, Y. Wang, S. Chen, and K. Li, "Dynamic eco-driving speed guidance at signalized intersections: multivehicle driving simulator based experimental study," *Journal of Advanced Transportation*, vol. 2018, Article ID 6031764, 11 pages, 2018.
- [16] F. Ma, Y. Yang, J. Wang et al., "Eco-driving-based cooperative adaptive cruise control of connected vehicles platoon at signalized intersections," *Transportation Research Part D: Transport and Environment*, vol. 92, Article ID 102746, 2021.
- [17] C. J. Hill and J. K. Garrett, "AASHTO connected vehicle infrastructure deployment analysis," *United States Joint Program Office for Intelligent Transportation Systems*, vol. 25, 2011.
- [18] H. Jiang, J. Hu, S. An, M. Wang, and B. B. Park, "Eco approaching at an isolated signalized intersection under partially connected and automated vehicles environment," *Transportation Research Part C: Emerging Technologies*, vol. 79, pp. 290–307, 2017.
- [19] Z. Wang, G. Wu, and M. J. Barth, "Cooperative eco-driving at signalized intersections in a partially connected and automated vehicle environment," *IEEE Transactions on Intelligent Transportation Systems*, vol. 21, no. 5, pp. 2029–2038, 2020.
- [20] W. Zhao, D. Ngoduy, S. Shepherd, R. Liu, and M. Papageorgiou, "A platoon based cooperative eco-driving model for mixed automated and human-driven vehicles at a signalised intersection," *Transportation Research Part C: Emerging Technologies*, vol. 95, pp. 802–821, 2018.
- [21] J. Hu, M. Lei, H. Wang, M. Wang, C. Ding, and Z. Zhang, "Lane-level navigation based eco-approach," *IEEE Transactions on Intelligent Vehicles*, vol. 8, no. 4, pp. 2786–2796, 2023.
- [22] J. Hu, Z. Zhang, L. Xiong, H. Wang, and G. Wu, "Cut through traffic to catch green light: eco approach with overtaking

- capability,” *Transportation Research Part C: Emerging Technologies*, vol. 123, Article ID 102927, 2021.
- [23] Y. Zhao, S. Yao, H. Shao, and T. Abdelzaher, “Codrive: cooperative driving scheme for vehicles in urban signalized intersections,” in *Proceedings of the 2018 ACM/IEEE 9th International Conference on Cyber-Physical Systems (ICCPS)*, pp. 308–319, Porto, Portugal, June 2018.
- [24] Z. Zhang and Y. Zou, “Green light optimal speed advisory system designed for electric vehicles considering queuing effect and driver,” *IEEE Access*, vol. 8, 2020.
- [25] H. Yang, H. Rakha, and M. V. Ala, “Eco-cooperative adaptive cruise control at signalized intersections considering queue effects,” *IEEE Transactions on Intelligent Transportation Systems*, vol. 18, no. 6, pp. 1–11, 2016.
- [26] R. Tu, L. Alfaseeh, S. Djavadian, B. Farooq, and M. Hatzopoulou, “Quantifying the impacts of dynamic control in connected and automated vehicles on greenhouse gas emissions and urban NO₂ concentrations,” *Transportation Research Part D: Transport and Environment*, vol. 73, pp. 142–151, 2019.
- [27] J. Yang, “Eco-driving of general mixed platoons with cavs and hdvs,” *IEEE Transactions on Intelligent Vehicles*, vol. 41, 2022.
- [28] T. Xiaofeng, “Ecological driving on multiphase trajectories and multiobjective optimization for autonomous electric vehicle platoon,” *Scientific Reports*, vol. 12, no. 1, p. 5209, 2022.
- [29] X. Li, A. Ghiasi, Z. Xu, and X. Qu, “A piecewise trajectory optimization model for connected automated vehicles: exact optimization algorithm and queue propagation analysis,” *Transportation Research Part B: Methodological*, vol. 118, pp. 429–456, 2018.
- [30] Z. Wang, G. Wu, P. Hao, and M. J. Barth, “Cluster-wise cooperative eco-approach and departure application for connected and automated vehicles along signalized arterials,” *IEEE Transactions on Intelligent Vehicles*, vol. 3, no. 4, pp. 404–413, 2018.
- [31] G. Yang, M. Ahmed, S. Gaweesh, and E. Adomah, “Connected vehicle real-time traveler information messages for freeway speed harmonization under adverse weather conditions: trajectory level analysis using driving simulator,” *Accident Analysis and Prevention*, vol. 146, Article ID 105707, 2020.
- [32] X. Chang, H. Li, J. Rong, Z. Huang, X. Chen, and Y. Zhang, “Effects of on-board unit on driving behavior in connected vehicle traffic flow,” *Journal of Advanced Transportation*, vol. 2019, Article ID 8591623, 12 pages, 2019.
- [33] J. A. Laval, “Self-organized criticality of traffic flow: implications for congestion management technologies,” *Transportation Research Part C: Emerging Technologies*, vol. 149, Article ID 104056, 2023.
- [34] K. Nagel and M. Paczuski, “Emergent traffic jams,” *Physical Review A*, vol. 51, no. 4, pp. 2909–2918, 1995.
- [35] K. Goldmann and G. Sieg, “Economic implications of phantom traffic jams: evidence from traffic experiments,” *Transportation Letters*, vol. 12, no. 6, pp. 386–390, 2020.
- [36] L. An, X. Yang, and J. Hu, “Modeling system dynamics of mixed traffic with partial connected and automated vehicles,” *IEEE Transactions on Intelligent Transportation Systems*, vol. 23, no. 9, pp. 15755–15764, 2022.
- [37] G. F. Newell, “A simplified theory of kinematic waves in highway traffic, part I: general theory,” *Transportation Research Part B: Methodological*, vol. 27, no. 4, pp. 281–287, 1993.
- [38] W.-L. Jin and J. Laval, “Bounded acceleration traffic flow models: a unified approach,” *Transportation Research Part B: Methodological*, vol. 111, pp. 1–18, 2018.
- [39] J. Lai, J. Hu, L. Cui, Z. Chen, and X. Yang, “A generic simulation platform for cooperative adaptive cruise control under partially connected and automated environment,” *Transportation Research Part C: Emerging Technologies*, vol. 121, Article ID 102874, 2020.
- [40] Y. Feng, K. L. Head, S. Khoshmagham, and M. Zamanipour, “A real-time adaptive signal control in a connected vehicle environment,” *Transportation Research Part C: Emerging Technologies*, vol. 55, pp. 460–473, 2015.
- [41] J. Lents and N. Nikkila, “IVE model user manual (version 1.1.1),” *International Sustainable Systems Research Center (ISSRC)*, EUA, La Habra, CA, USA, 2004.
- [42] H. Liu, K. He, and M. Barth, “Traffic and emission simulation in China based on statistical methodology,” *Atmospheric Environment*, vol. 45, no. 5, pp. 1154–1161, 2011.
- [43] H. Xia, *Eco-Approach and Departure Techniques for Connected Vehicles at Signalized Traffic Intersections*, University of California, Riverside, CA, USA, 2014.